applied sciences

MDPI

Article

Modified Extended Complex Kalman Filter for DC Offset and Distortion Rejection in Grid-Tie Transformerless Converters

Mohammed El-Nagar [1,*], Khaled Ahmed [2], Eman Hamdan [3], Ayman S. Abdel-Khalik [1], Mostafa S. Hamad [4] and Shehab Ahmed [5]

[1] Electrical Engineering Department, Faculty of Engineering, Alexandria University, Alexandria 21544, Egypt; ayman.abdel-khalik@alexu.edu.eg
[2] Department of Electronic and Electrical Engineering, University of Strathclyde, Glasgow G1 1XQ, UK; khaled.ahmed@strath.ac.uk
[3] Marine Engineering Technology Department, Arab Academy for Science, Technology and Maritime Transport, Alexandria 21913, Egypt; eman_youssef@aast.edu
[4] Electrical and Control Engineering Department, Arab Academy for Science, Technology and Maritime Transport, Alexandria 21913, Egypt; mostafa.hamad@staff.aast.edu
[5] CEMSE Division, King Abdullah University of Science and Technology, Thuwal 23955, Saudi Arabia; shehab.ahmed@kaust.edu.sa
* Correspondence: mohammed.elnagar@alexu.edu.eg

Abstract: Proper operation of the grid-tie transformerless converters under unbalanced and distorted conditions entails a precise detection of the frequency and fundamental component of the grid voltage. One of the main problems that could arise during the estimation of grid parameters is the existence of a DC offset generated from measurement and A/D conversion. This undesirable induced DC offset could appear as a part of the reference sinusoidal current of grid-tie converters. Although literature has proposed the use of an extended complex Kalman filter (ECKF) for the estimation of positive and negative sequence voltage components as a promising competitor to phase locked loops, mitigating the effect of possible DC offsets when a Kalman filter is employed remains scarce. This paper proposes a new extended complex Kalman filter to improve the filter stability for estimating the frequency and the fundamental positive and negative symmetrical components of the grid voltages, where DC offset, scaling error, and noise can successfully be rejected. The theoretical findings are experimentally validated.

Keywords: extended complex Kalman filter; grid-tie converter; DC offset and scaling errors; harmonic mitigation

Citation: El-Nagar, M.; Ahmed, K.; Hamdan, E.; Abdel-Khalik, A.S.; Hamad, M.S.; Ahmed, S. Modified Extended Complex Kalman Filter for DC Offset and Distortion Rejection in Grid-Tie Transformerless Converters. *Appl. Sci.* **2023**, *13*, 9023. https://doi.org/10.3390/app13159023

Academic Editor: Juan P. Torreglosa

Received: 29 June 2023
Revised: 26 July 2023
Accepted: 28 July 2023
Published: 7 August 2023

1. Introduction

It is crucial to know the phase angle, frequency, and amplitude of grid voltage in order to properly operate and control a variety of grid-tie converters, including photovoltaic (PV) converters, pulse width modulation rectifiers, uninterrupted power supplies (UPSs), distributed power systems, and others. This process is commonly known as grid synchronization [1–7]. A precise and quick algorithm is required to measure the symmetrical components, particularly in a harmonically contaminated, unbalanced three-phase system. When estimating the grid characteristics, particular attention should be paid to the presence of possible DC offsets in the observed grid voltage. Voltage sensing, filtering, and A/D conversion are generally the three functions that the grid interface circuit should carry out. Even if the grid interface circuit is correctly constructed, the non-linearity of voltage sensors, A/D conversion, and thermal drift of analog components commonly yields DC offsets in measured grid voltages [8]. Typically, the maximum allowable dc current injection in a grid-tie converter should not exceed 0.5% of the full rated output current at the point of common coupling [9].

Three main categories can be used to group the techniques for suppressing dc current injection: blocking dc current with a capacitor [10,11], voltage (and/or) current detection control [12–18], and innovative converter topologies with dc current suppression capabilities [19–21]. However, the first strategy requires a bulky and expensive capacitor and may produce extra losses and poor power quality. Moreover, the dynamic response and system stability have been affected when the virtual capacitor technique is used [11]. Additionally, the grid distortion and the scaling errors in the measured grid voltages continue to have an impact on the grid current performance under this strategy [22]. On the contrary, the detection strategy may increase the system footprint, increasing cost and power loss [23]. In fact, this strategy has been frequently employed in motor drive applications for compensating the errors in measured currents [14,19–21,23,24]. However, there are major challenges when applying this technique to grid-tie converter applications because measurement errors might occur on both current and voltage signals, leading to inaccurate compensation results if only current or voltage measurement errors are compensated [22]. In the third strategy, current controllers with the ability to reject DC offsets have been introduced. This method seems to be simpler to practically implement since the DC offset and the scaling error in measured voltages do not need to be detected or estimated. Several converter control techniques are used to estimate positive and negative fundamental components from unbiased and unbalanced three-phase signals based on phase-locked loop implementation [25–30]. However, there are challenges facing the design of PLL, such as instability problems [31–34], complexity in the case of abnormal grid conditions [35], and a large calculation burden [36].

In [37], the positive sinusoidal signal in a grid with white noise is estimated using the extended complex Kalman filter (ECKF). Using Kalman filter algorithms, the works in [38–40] have suggested determining the power frequency in distorted grids based on their estimated sequence components. The concept of employing a modified Kalman filter to make up for the DSP computation delay is covered in [41]. To estimate the symmetrical components from unbalanced grid voltages without a PLL, the ECKF suggested in [42] is applied. As a result, as compared to previous methods, better noise rejection has been obtained while avoiding tuning and delay concerns. In [43], authors presented a new space vector-based model predictive current controller to deal with unbalanced and distorted grid conditions. The current references in this model-predictive algorithm are computed based on symmetrical fundamental components of grid voltages. The important note is the use of the conventional ECKF to estimate these sequence voltages. The prior methods, however, have not been investigated under biased, unbalanced, and distorted scenarios.

The main contributions of this paper are summarized in the following bullets:

- A modified extended complex Kalman filter is presented to improve the filter's performance for estimating symmetrical components in the presence of DC offset and noise.
- Harmonic free current references are calculated based on the estimated positive and negative symmetrical components of grid voltages for both ECKF strategies. The finite control set model predictive control (FCS-MPC) current control structure is presented such that the grid currents follow exactly the pure sinusoidal current references generated by the current reference generator.
- The principle of FCS-MPC is to drive the converter switches by minimizing the cost function without the need for PWM techniques. As a result, FCS_MPC features a simple real-time hardware implementation, a quick response, a higher stability margin, and the ability to handle of multiple objectives and nonlinear constraints [44].

The paper is organized as follows: Section 2 describes the problem statement. Section 3 presents the mathematical model of conventional ECKF and also presents the proposed ECKF. In Section 4, the simulation results are presented using MATLAB/SIMULINK 9.4 (R2018a) software to validate the effectiveness of the proposed ECKF over the conventional one under DC offset and distorted conditions. Section 5 includes the experimental validation of the proposed ECKF.

2. Problem Statement

There are typically no even or triplen harmonics in three-phase power systems; as a result, the three-phase grid voltages only contain the harmonic component $h = 6n \mp 1$ (n = 1, 2, 3, ...).

$$v_{gj} = \mathrm{V}_1 \cos\left(\omega_s t - (i-1)\frac{2\pi}{3}\right) + \sum_{n=1}^{\infty} \mathrm{V_h} \cos\left((6n \mp 1)\left(\omega_s t - (i-1)\frac{2\pi}{3}\right)\right) \quad (1)$$

V_1 and $\mathrm{V_h}$ are the amplitudes of fundamental and harmonic components, respectively, $j \in \{a, b, c\}$, $i = 1,\ 2,$ and 3 for $j = a$, b, and c, respectively, and ω_s is the fundamental angular frequency of the grid.

Monitoring three-phase grid voltages using some type of amplifier circuits and, hence, implementing digital readings using the analog-to-digital conversion (ADC) module of the microcontroller are preliminary steps in the control algorithm of the grid-tie converter. Assuming that voltage measurement readings include scaling and DC offset errors, the three-phase grid voltages measured by the microcontroller can be expressed as follows:

$$v_{gj}^{ADC} = (1 - \Delta k_j) v_{gj} + V_{js}; \quad j \in \{a, b, c\} \quad (2)$$

According to (2), v_{ga}^{ADC}, v_{gb}^{ADC}, and v_{gc}^{ADC} are the digital readings of the three-phase grid voltage a, b, and c, respectively; Δk_a, Δk_b, and Δk_c are the scaling errors for each phase a, b, and c respectively; V_{as}, V_{bs}, and V_{cs} are the DC offsets in the measurements. Applying Clarke's transformation, the stationary $\alpha\beta$ components of the grid voltages ($v_{g\alpha}$ and $v_{g\beta}$) are obtained and contain DC offset and AC ripple at ω_s and $(6n \mp 1)\omega_s$ (n = 1, 2, 3, ...). The DC component of the grid voltages can be given by:

$$v_{g\alpha}^{DC} = V_{as} - \frac{1}{2}(V_{bs} + V_{cs}) \quad (3)$$

$$v_{g\beta}^{DC} = \frac{\sqrt{3}}{2}(V_{bs} - V_{cs}) \quad (4)$$

The stationary $\alpha\beta$ components of converter voltages ($v_{c\alpha}$ and $v_{c\beta}$) are then given by (5), where i_α and i_β are the stationary $\alpha\beta$ components of output currents.

$$\begin{bmatrix} v_{c\alpha} \\ v_{c\beta} \end{bmatrix} = \begin{bmatrix} v_{g\alpha} \\ v_{c\beta} \end{bmatrix} + R \begin{bmatrix} i_\alpha \\ i_\beta \end{bmatrix} + L \begin{bmatrix} \frac{di_\alpha}{dt} \\ \frac{di_\beta}{dt} \end{bmatrix} \quad (5)$$

As the terms $v_{g\alpha}$ and $v_{g\beta}$ contain DC offset and AC ripple at ω_s and $(6n \mp 1)\omega_s$ (n = 1, 2, 3, ...), they subsequently inject undesired DC and AC ripple at the same frequencies into i_α and i_β. There is a need to present a current controller by which the DC offset and distortion are rejected.

3. Mathematical Modelling

3.1. Conventional Extended Complex Kalman Filter

Let a noisy distorted signal z_k of h negative and positive sinusoids be given by:

$$z_k = \sum_{i=1}^{h} \mathrm{A_i^+} \mathrm{e}^{j(\omega_i TK + \phi_i^+)} + \mathrm{A_i^-} \mathrm{e}^{-j(\omega_i TK + \phi_i^-)} + \mathrm{Noise} \quad (6)$$

$\mathrm{A_i^+}$ and $\mathrm{A_i^-}$ are the amplitudes of positive and negative sinusoids, ω_i is the angular frequency, ϕ_i^+ and ϕ_i^- are the phase angles of the positive and negative sinusoid, respectively, and T is the sampling time.

To model the observation signal y_k, the state space representation is given by:

$$x_{k+1} = f(x_k) = A\, x_k \quad (7)$$

$$y_k = Hx_k + v_k \tag{8}$$

where (9) and (10) are given as follows:

$$\begin{bmatrix} \gamma \\ x_{1(k+1)} \\ x_{2(k+1)} \end{bmatrix} = \begin{bmatrix} 1 & 0 & 0 \\ 0 & \gamma & 0 \\ 0 & 0 & \gamma^{-1} \end{bmatrix} \begin{bmatrix} \gamma \\ x_{1(k)} \\ x_{2(k)} \end{bmatrix} \tag{9}$$

$$[y_k] = \begin{bmatrix} 0 & 1 & 1 \end{bmatrix} \begin{bmatrix} \gamma \\ x_{1(k)} \\ x_{2(k)} \end{bmatrix} + [v_k] \tag{10}$$

where

$$\gamma = \exp(j\omega_s T) \tag{11}$$

$$x_{1(k)} = \mathrm{A_i^+ e}^{j(\omega_s TK + \phi_1^+)} \tag{12}$$

$$x_{2(k)} = \mathrm{A_i^- e}^{-j(\omega_s TK + \phi_1^-)} \tag{13}$$

The artificial state γ expresses the variation in the fundamental frequency. $x_{1(k)}$ is the recent state of the positive fundamental component, and $x_{2(k)}$ is the recent state of the negative fundamental component of the grid voltages.

Applying the following ECKF algorithm [37]:

$$K_k = \hat{P}_{k|k-1}\, H^H \left(H\hat{P}_{k|k-1}\, H^H + R \right)^{-1} \tag{14}$$

$$\hat{x}_{k|k} = \hat{x}_{k|k-1} + K_k \left(y_k - H\hat{x}_{k|k-1} \right) \tag{15}$$

$$\hat{P}_{k|k} = (I - K_k\, H\,)\, \hat{P}_{k|k-1} \tag{16}$$

$$\hat{x}_{k+1|k} = A\, \hat{x}_{k|k} \tag{17}$$

$$\hat{P}_{k+1|k} = F\hat{P}_{k|k}\, F^H + Q \tag{18}$$

where

$$F = \frac{df(x_k)}{dx_k}_{|x_k = \hat{x}_{k|k}} = \begin{bmatrix} 1 & 0 & 0 \\ \hat{x}_{1k|x} & \hat{\gamma} & 0 \\ -\hat{\gamma}^{-2} \cdot \hat{x}_{2k|x} & 0 & \hat{\gamma}^{-1} \end{bmatrix} \tag{19}$$

F, H are the linearized transition and measurement matrices, and F^H, H^H are the Hermitian of these matrices, respectively. Moreover, the observation and process noise covariance matrices are R and Q; the estimated state is denoted by x; P denotes the state error covariance matrix, whereas Kalman gain is represented by notation K_k.

It is worth noting that any decrease in Kalman gain causes the filter to more closely match model predicted states, whereas the most recent measurements are given more weight whenever the Kalman gain increases. To obtain the best performance, R and Q are experimentally tuned.

The estimated state one step in advance $\hat{x}_{k+1}$ can be given based on the recent state $\hat{x}_k$ by (20).

$$\hat{x}_{k+1} = A\, \hat{x}_k \tag{20}$$

Moreover, the advance of states by two steps can be given by:

$$\hat{x}_{k+2} = A\, \hat{x}_{k+1} \tag{21}$$

Noting that

$$x_{1(k)} = V^{+}_{g\alpha\beta} = V^{+}_{g\alpha(k)} + jV^{+}_{g\beta(k)} \tag{22}$$

$$x_{2(k)} = V^{-}_{g\alpha\beta} = V^{-}_{g\alpha(k)} + jV^{-}_{g\beta(k)} \tag{23}$$

3.2. Modified Extended Complex Kalman Filter

A modified extended complex Kalman filter is proposed to achieve DC offset and noise rejection.

Unlike conventional ECKF, where its output states are expected to contain DC components, the modified ECKF uses state feedback loops to remove the expected DC offsets.

Define two observation signals as shown in Figure 1. The first observation signal $y_{1(k)}$ is the distorted signal z_k extracted from it, the fundamental negative signal $x_{2(k)}$. The observation signal $y_{2(k)}$ is the distorted signal z_k extracted from it, the fundamental positive signal $x_{1(k)}$.

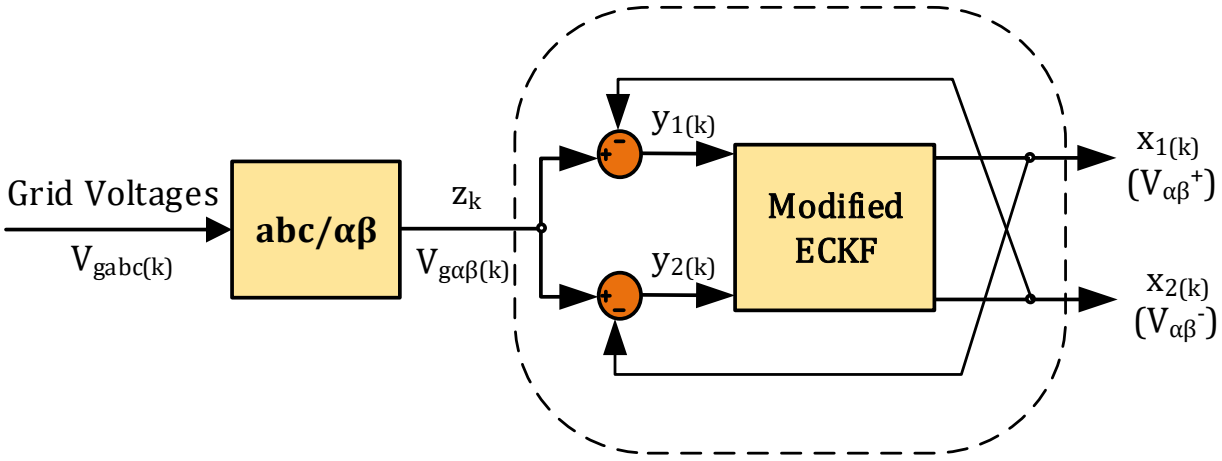

Figure 1. The modified extended complex Kalman filter.

To model the observation signals $y_{1(k)}$ and $y_{2(k)}$, the state space representation can be given by (9), while (10) is replaced by (24).

$$\begin{bmatrix} y_{1(k)} \\ y_{2(k)} \end{bmatrix} = \begin{bmatrix} 0 & 1 & 0 \\ 0 & 0 & 1 \end{bmatrix} \begin{bmatrix} \gamma \\ x_{1(k)} \\ x_{2(k)} \end{bmatrix} + \begin{bmatrix} v_{1(k)} \\ v_{2(k)} \end{bmatrix} \tag{24}$$

On the other hand, Equations (11)–(23) remain the same. In conclusion, the method suggests that the DC component in the input distorted signal is subtracted before the ECKF algorithm is applied.

4. Current Control Structure

A block diagram of the FCS-MPC current control structure based on the ECKF estimator is presented in Figure 2 to improve the output grid currents of the grid-tie PV transformerless converter.

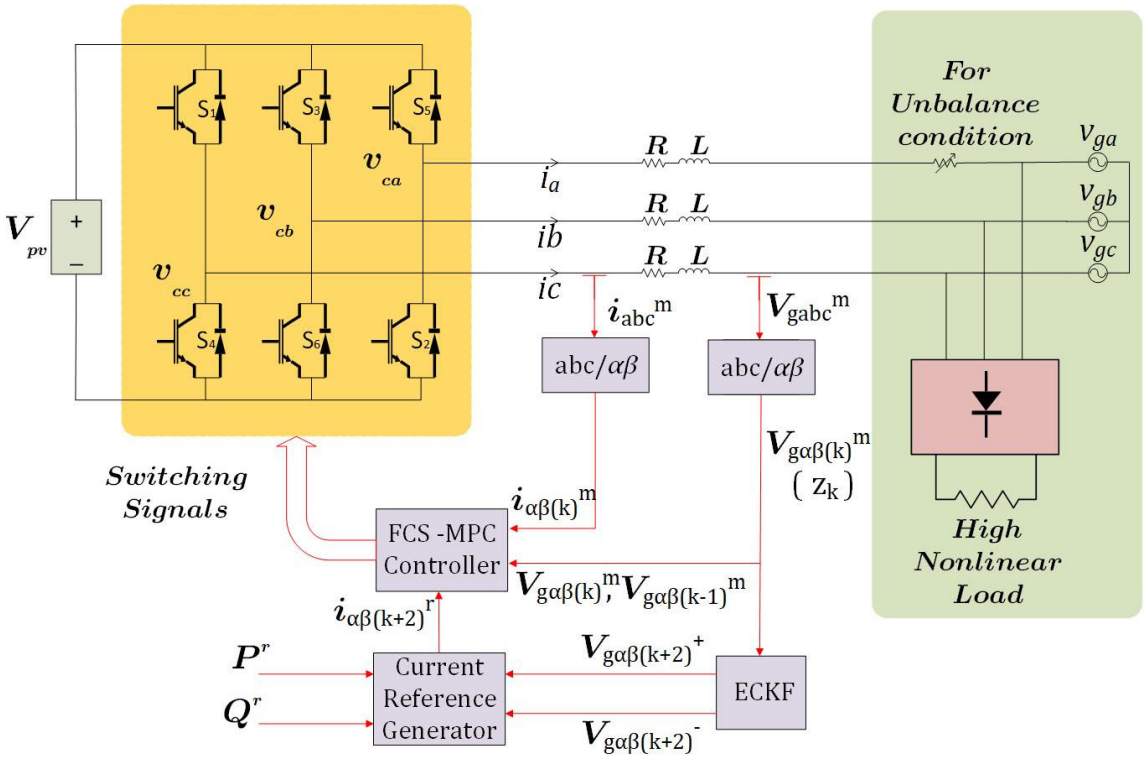

Figure 2. Block diagram of grid-tie PV converter with FCS-MPC current control structure.

Considering the dynamic equation of the grid-tie transformerless voltage source converter interfaced via an L filter is discussed (R and L are the resistance and inductance of the filter), it is given in the stationary $\alpha\beta$ reference frame by (25). Based on the forward Euler discretization rule in (26), the discrete predictive current model can be expressed by (27). In (27), the assumption that the grid voltages at a recent instant are the same as the last instant is acceptable. The reason is that the periodic time of the grid voltage waveform is much longer than the sampling time.

$$L\begin{bmatrix}\frac{di_\alpha}{dt}\\ \frac{di_\beta}{dt}\end{bmatrix} = \begin{bmatrix}v_{c\alpha}\\ v_{c\beta}\end{bmatrix} - \begin{bmatrix}v_{g\alpha}\\ v_{c\beta}\end{bmatrix} - R\begin{bmatrix}i_\alpha\\ i_\beta\end{bmatrix} \tag{25}$$

$$\frac{di}{dt} = \frac{i_{(k+1)} - i_{(k)}}{T_s} \tag{26}$$

$$\begin{bmatrix}i_{\alpha(k+1)}\\ i_{\beta(k+1)}\end{bmatrix} = \frac{T_s}{L}\begin{bmatrix}V_{c\alpha(k)} - V_{g\alpha(k-1)}\\ V_{c\beta(k)} - V_{g\beta(k-1)}\end{bmatrix} + (1 - \frac{R\,T_s}{L})\begin{bmatrix}i_{\alpha(k)}\\ i_{\beta(k)}\end{bmatrix} \tag{27}$$

To compensate for the control action delay, the current model two steps in advance is predicted as follows:

$$\begin{bmatrix}i_{\alpha(k+2)}\\ i_{\beta(k+2)}\end{bmatrix} = \frac{T_s}{L}\begin{bmatrix}V_{c\alpha(k+1)} - V_{g\alpha(k)}\\ V_{c\beta(k+1)} - V_{g\beta(k)}\end{bmatrix} + \left(1 - \frac{R\,T_s}{L}\right)\begin{bmatrix}i_{\alpha(k+1)}\\ i_{\beta(k+1)}\end{bmatrix} \tag{28}$$

As a result, the current references are calculated based on (29)–(32) to suppress active power 2nd order oscillations depending on the estimated positive and negative fundamental components [43].

$$\begin{bmatrix} i^r_{\alpha(k+2)} \\ i^r_{\beta(k+2)} \end{bmatrix} = \begin{bmatrix} 1 & 0 & 1 & 0 \\ 0 & 1 & 0 & 1 \end{bmatrix} \begin{bmatrix} i^+_{\alpha(k+2)} \\ i^+_{\beta(k+2)} \\ i^-_{\alpha(k+2)} \\ i^-_{\beta(k+2)} \end{bmatrix} \tag{29}$$

where

$$\begin{bmatrix} i^+_{\alpha(k+2)} \\ i^+_{\beta(k+2)} \\ i^-_{\alpha(k+2)} \\ i^-_{\beta(k+2)} \end{bmatrix} = \begin{bmatrix} \frac{V^+_{g\alpha(k+2)}}{C} & \frac{V^+_{g\beta(k+2)}}{D} \\ \frac{V^+_{g\beta(k+2)}}{C} & -\frac{V^+_{g\beta(k+2)}}{C} \\ -\frac{V^-_{g\alpha(k+2)}}{C} & \frac{V^-_{g\beta|k+1}}{C} \\ -\frac{V^-_{g\beta(k+2)}}{C} & -\frac{V^-_{g\alpha(k+2)}}{C} \end{bmatrix} \begin{bmatrix} P^r \\ Q^r \end{bmatrix} \tag{30}$$

and,

$$C = {V^+_{g\alpha(k+2)}}^2 - {V^-_{g\alpha(k+2)}}^2 + {V^+_{g\beta(k+2)}}^2 - {V^-_{g\beta(k+2)}}^2 \tag{31}$$

$$D = {V^+_{g\alpha(k+2)}}^2 + {V^-_{g\alpha(k+2)}}^2 + {V^+_{g\beta(k+2)}}^2 + {V^-_{g\beta(k+2)}}^2 \tag{32}$$

The switching signals corresponding to the optimal voltage vector are obtained such that the smallest value of the cost function in (33) is achieved:

$$G = \left[i^r_{\alpha(k+2)} - i_{\alpha(k+2)} \right]^2 + \left[i^r_{\beta(k+2)} - i_{\beta(k+2)} \right]^2 \tag{33}$$

5. Simulation Results

The conventional and proposed modified ECKF algorithms are investigated under biased, unbalanced, and distorted conditions.

A positive fundamental grid reference component (V_g^+) with 100 V amplitude is considered. The voltage unbalance factor (V_{UF}) is given by (34), where V_g^- is the negative fundamental grid reference component. A value of V_{UF} is chosen to be 20%. The grid distortion is considered by adding 5th and 7th harmonics of 12% and 8% of the reference, respectively.

$$V_{UF} = \frac{V_g^-}{V_g^+} \times 00\% \tag{34}$$

White noise is added as presented in Figure 3. The reference *abc* grid voltages are transformed using Clarke's transformation into reference $\alpha\beta$ grid components and fed to the ECKF input in the complex form (z_k). Moreover, significant DC offsets (V_{as}, V_{bs}, and V_{cs}) are applied at percentages of 70%, 50%, and 30%, respectively, of the peak value of the positive fundamental component at instant 0.04 s. The per unit (p.u.) *abc* grid voltages and the fundamental positive and negative $\alpha\beta$ components are illustrated in Figure 3 in the case of conventional and proposed ECKF.

In Figure 4, the output fundamental positive and negative $\alpha\beta$ components are transformed into fundamental positive and negative *abc* components and compared with the reference positive and negative *abc* grid voltages for detailed documentation.

Moreover, the grid fundamental frequency under both algorithms is estimated using (35) and is introduced in Figure 5, where the reference is 50 Hz.

$$f_s = \ln\left(\frac{Imag(\gamma)}{2\pi T} \right) \tag{35}$$

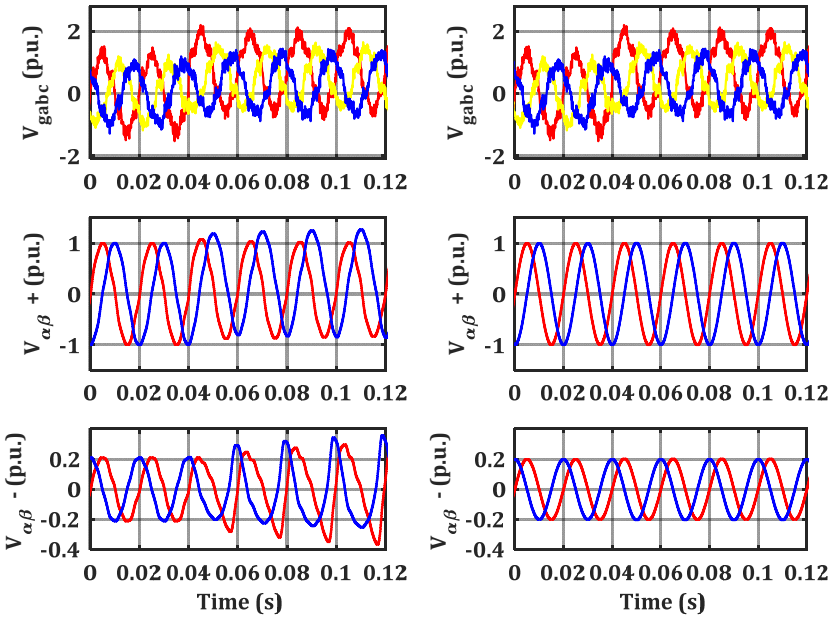

Figure 3. The *abc* grid voltages, positive and negative fundamental $\alpha\beta$ components in case of (**a**) conventional ECKF, and (**b**) modified ECKF.

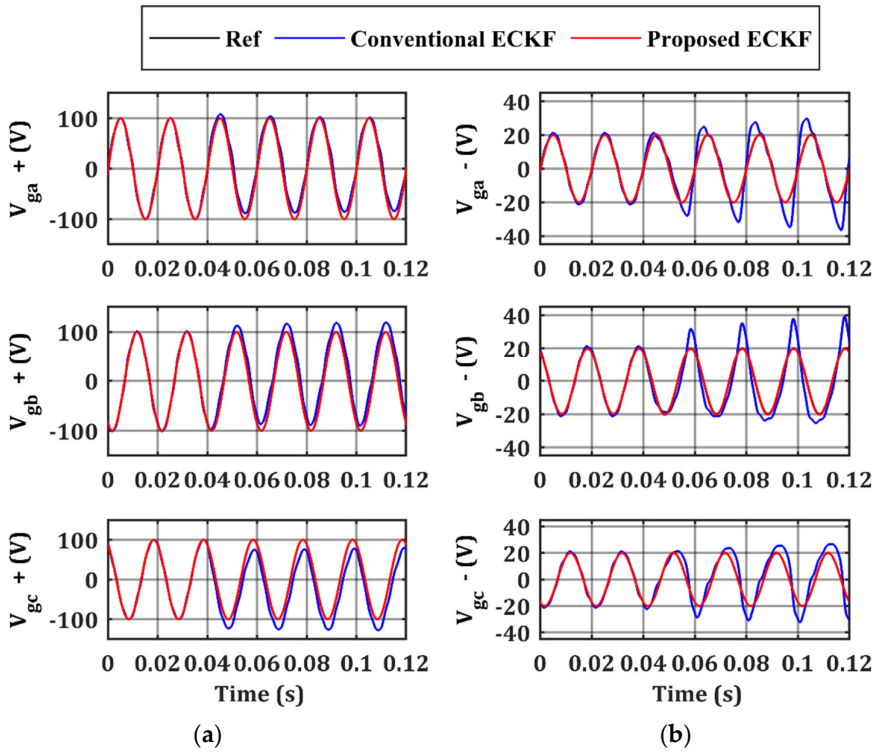

Figure 4. The reference and the estimated values of positive and negative components of grid phases *a*, *b*, and *c* grid voltages in case of (**a**) conventional ECKF, and (**b**) modified ECKF.

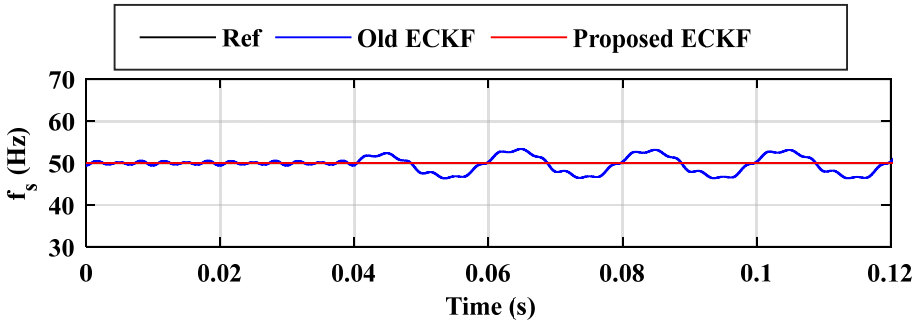

Figure 5. The reference and the estimated grid fundamental frequency in case of conventional and modified ECKF.

According to the simulation results, both algorithms give correct estimation if the input signal is free of DC offset. However, the conventional ECKF leads to obvious offsets in estimated symmetrical components. Moreover, it behaves like oscillations in the estimated frequency in the case of a biased input signal. Based on the results, the priority of the proposed modified ECKF in estimating positive and negative fundamental components is ensured. In conclusion, it is expected that the proposed ECKF will provide harmonic-free current references, while the reference currents calculated based on the estimated values introduced by the conventional ECKF may be distorted.

6. Experimental Validation

The experimental setup of the grid-tie PV converter is shown in Figure 6. To investigate the conventional and the proposed ECKF under unbalanced and distorted conditions, series resistance is used to increase the phase voltage (v_{ga}) by 14% (unbalance condition), and a high nonlinear rectifier load is shunted with the phases on the AC grid side to produce voltage distortion (distorted behavior). The OP4510 real-time simulator with four digital and analog I/O modules is used with a clock frequency of 2.1 GHz. The IKCM30F60GD fully isolated voltage source converter module is combined with three LV 25-P voltage sensors and three LA 25-NP hall effect current sensors to interface with a three-phase programmable source via an L filter, as shown in Figure 6. A 100 V DC supply is used as the DC link voltage. Hence, the maximum AC grid voltage in this case will be 28 V rms. For more details, Table 1 presents the system parameters.

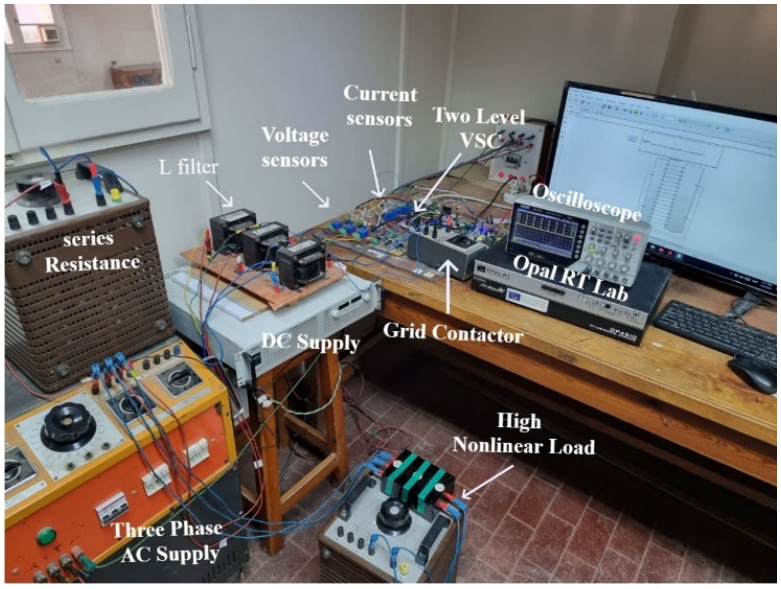

Figure 6. Experimental test setup.

Table 1. Hardware parameters.

Parameters	Symbol	Value (Unit)
Grid phase voltage (RMS)	v^m_{gabc}	28 V
Grid fundamental frequency	f_1	50 Hz
Switching frequency	f_{sw}	10 kHz
DC link voltage	V_{dc}	100 V
Filter Inductance	L	6.7 mH
Filter Resistance	R	1.6 Ω

Considering the measurement errors in Table 2, the grid voltages are biased, as shown in Figure 7. By applying the empirically determined values of the Kalman covariance matrices given by (36) and (37), the estimated positive fundamental $\alpha\beta$ components presented in Figure 8 behave more accurately using the modified ECKF compared with the conventional ECKF. On the other hand, the DC offsets and phase shift errors in the estimated negative $\alpha\beta$ components are obvious in the case of conventional ECKF, as illustrated in Figure 9. Consequently, a zoomed view is presented in Figure 10 to configure the reference currents calculated based on the estimated symmetrical components in the case of conventional ECKF or modified ECKF.

$$Q = \begin{bmatrix} 5e^{-17} & 0 & 0 \\ 0 & 5e^{-6} & 0 \\ 0 & 0 & 5e^{-6} \end{bmatrix} \tag{36}$$

$$R = [100] \tag{37}$$

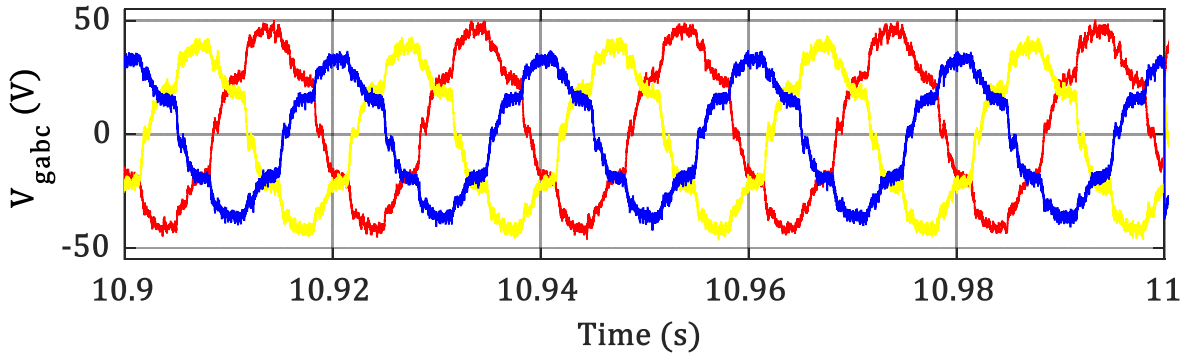

Figure 7. Three-phase grid voltages (unbalanced distorted conditions).

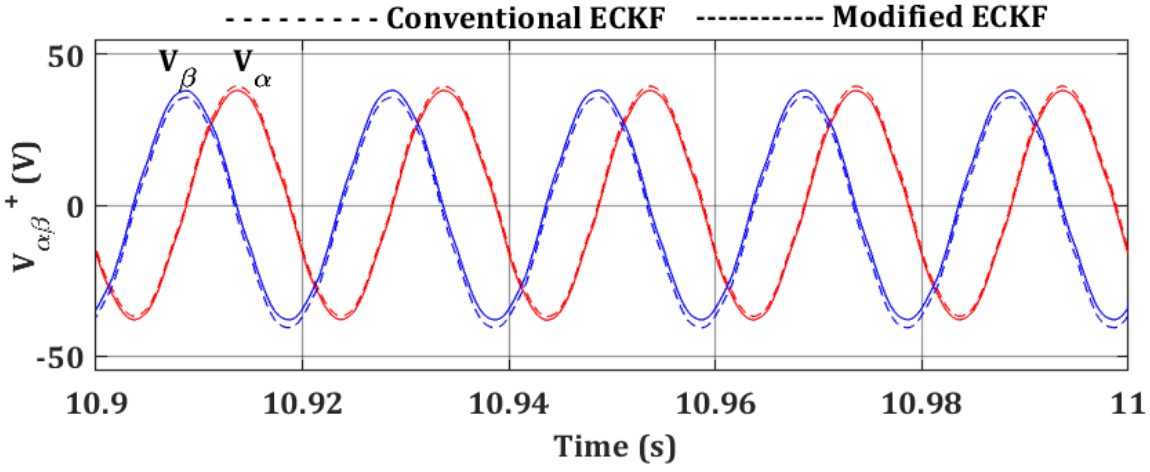

Figure 8. The estimated positive fundamental $\alpha\beta$ components in case of conventional and modified ECKF.

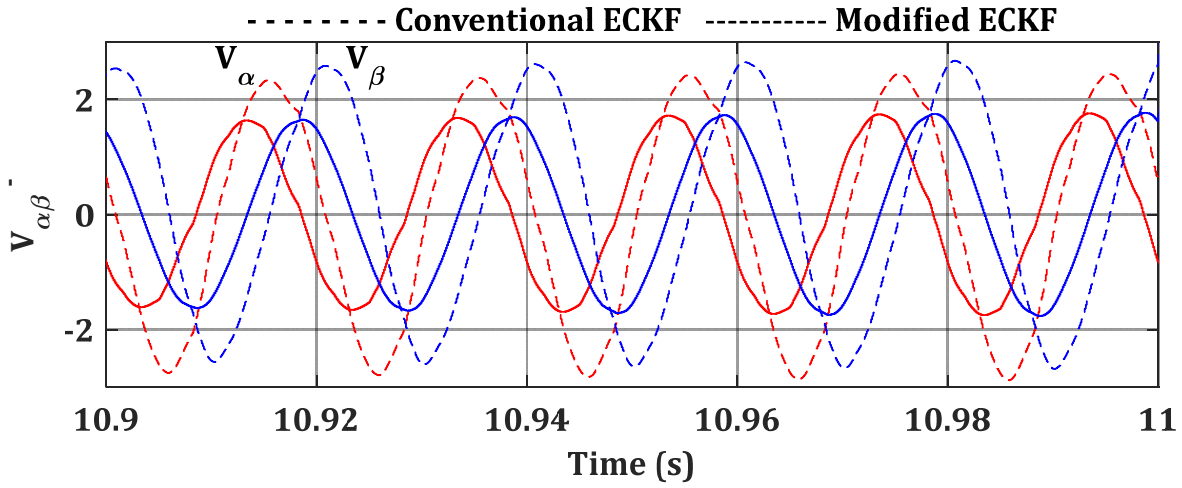

Figure 9. The estimated negative fundamental $\alpha\beta$ components in case of conventional and modified ECKF.

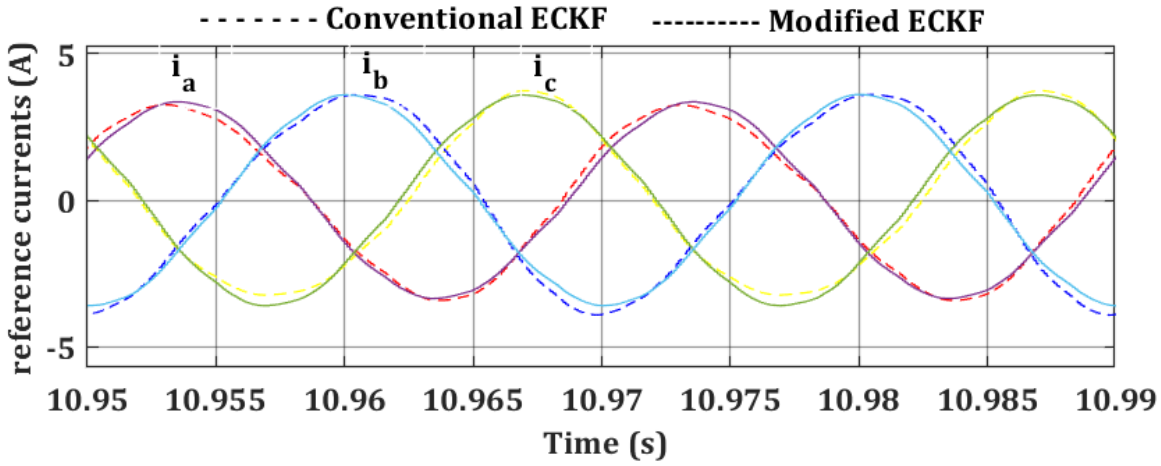

Figure 10. Zoomed view for the reference currents in case of conventional and modified ECKF.

Table 2. Scaling errors and measurement offsets.

Δk_a	−0.02	V_{as}	+2.5
Δk_b	−0.08	V_{bs}	−2
Δk_c	+0.08	V_{cs}	−1.5

To investigate the effectiveness of the modified ECKF over the conventional one, the frequency responses of the accompanying reference currents are presented in Figure 11. The main observation is the appearance of a 2nd order harmonic component in the case of conventional ECKF as a result of the false estimation of positive and negative components. Therefore, the total harmonic distortion (THD) in the case of modified ECKF is much smaller than that of the conventional ECKF.

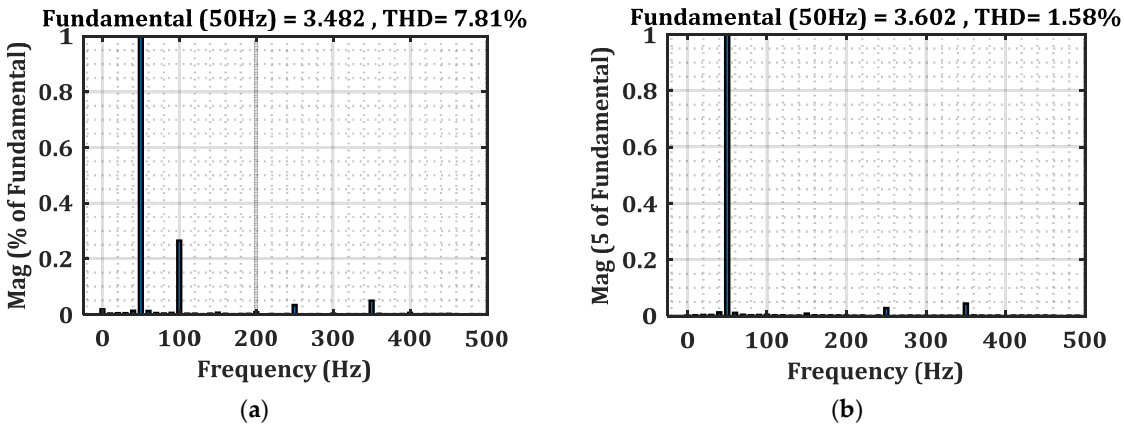

Figure 11. The frequency response of the reference currents in case of (**a**) conventional ECKF and (**b**) modified ECKF.

The three-phase grid currents are illustrated in Figures 12 and 13 in the case of conventional and modified ECKF, respectively. More smooth output currents are provided in the case of modified ECKF, as shown in Figure 13. Moreover, the modified ECKF offers a better estimation for the grid frequency, as shown in Figure 14. On the other side, the predicted grid frequency oscillates in the case of conventional ECKF.

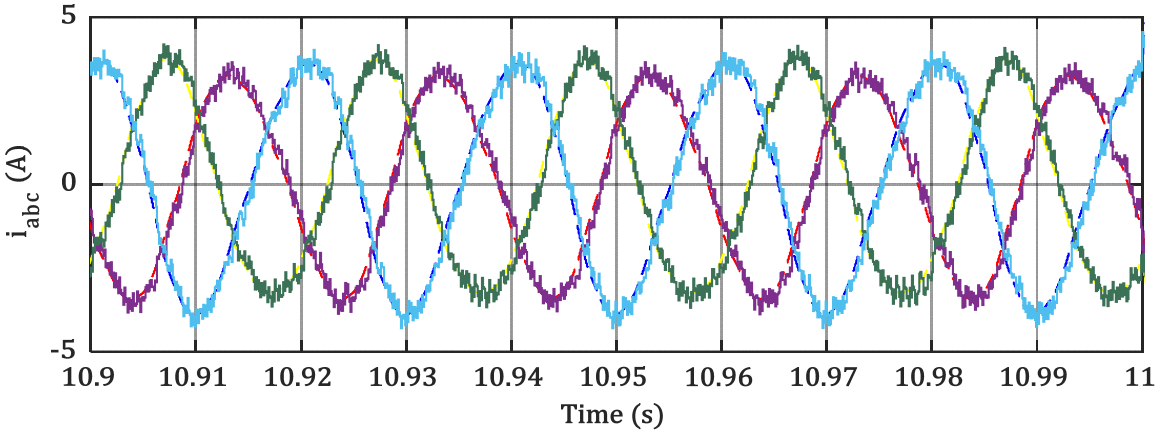

Figure 12. Three-phase grid currents in case of conventional ECKF. Phase *a* is in green colour, *b* is violet, and *c* is blue.

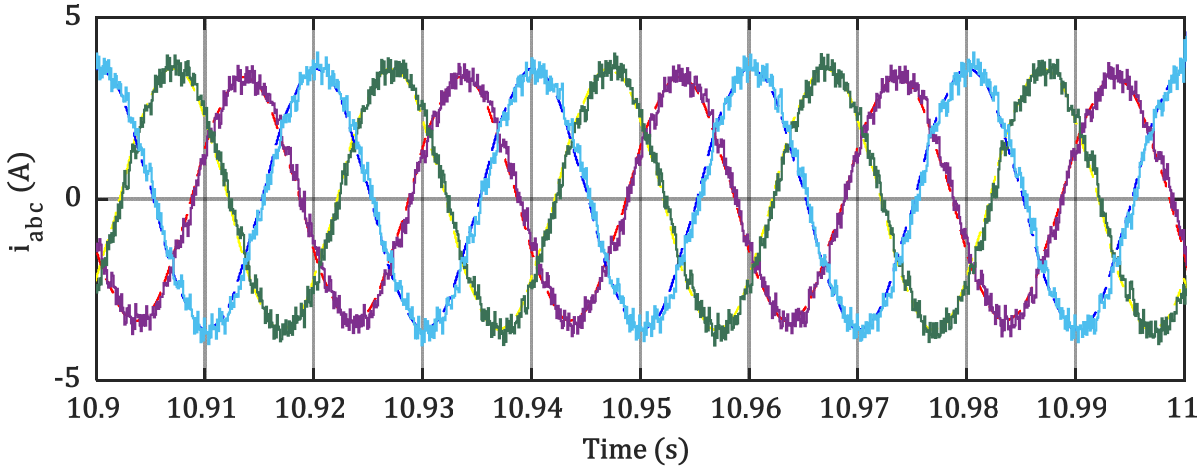

Figure 13. Three-phase grid currents in case of modified ECKF.

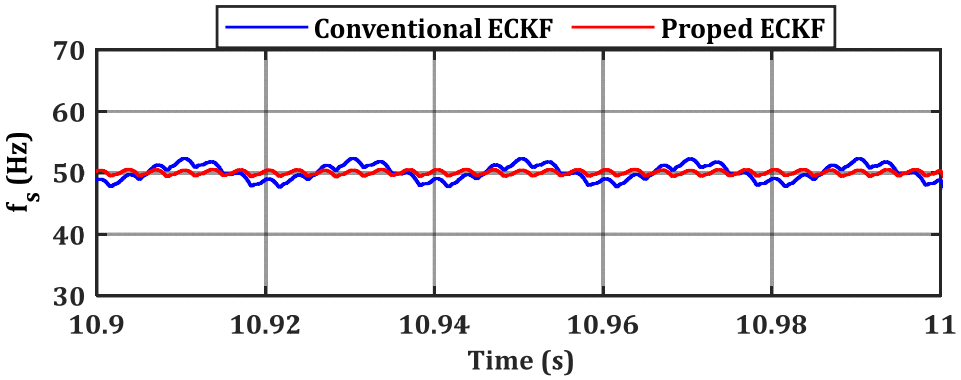

Figure 14. The estimated grid frequency in case of conventional and modified ECKF.

7. Discussion

The proposed technique ECKF has been introduced to estimate the sequence components of biased, unbalanced, and distorted grid voltages caused by the existence of DC offsets generated from the measurement and A/D conversion stages.

The simulation results show that the conventional ECKF provides a poor response compared with the modified ECKF in the case of biased grid voltages. In addition, an experimental setup is introduced where the FCS model predictive current controller is used and the reference currents are generated based on the positive and negative fundamental components estimated by using the conventional and modified ECKF. Experimental results have been introduced to validate the priority of the proposed ECKF over the conventional one in the case of unbalanced and distorted conditions. As illustrated in Table 3, the current THD in the case of modified ECKF is reduced by 80% compared with the conventional one.

Table 3. THD results.

Conventional ECKF		Modified ECKF		Reduction Percentage	
THD	7.81	THD	1.58	Reduction	80%

In general, the modified ECKF estimator achieves less total harmonic distortion and corrects current magnitudes and phase angles as compared with the conventional ECKF filter presented in the literature.

It is worth noting that this proposed ECKF is unable to deal with even harmonics due to possible nonlinearities and asymmetries, which are postponed for future work. This point can be useful for current tracking in grid-tie uncontrolled rectifier applications.

8. Conclusions

In this paper, the proposed ECKF filter has been introduced to estimate the positive and negative sequence components of biased, unbalanced, and distorted grid conditions of grid-tie transformerless converters while considering the existence of a DC offset generated from measurement and an A/D conversion. The proposed ECKF estimator presents better estimated results compared with the conventional ECKF used in the literature. The current harmonic distortion is reduced by 80% and, consequentially, yields a better performance in the overall current control structure.

Author Contributions: Conceptualization, M.E.-N.; methodology, M.E.-N., K.A. and A.S.A.-K.; software, M.E.-N.; validation, M.E.-N.; formal analysis, E.H. and M.S.H.; investigation, M.E.-N.; resources, A.S.A.-K.; data curation, M.E.-N., K.A. and A.S.A.-K.; writing—original draft preparation, M.E.-N.; writing—review and editing, M.E.-N. and A.S.A.-K.; visualization, M.E.-N.; supervision, M.E.-N., K.A. and A.S.A.-K.; project administration, K.A. and A.S.A.-K.; funding acquisition, S.A. All authors have read and agreed to the published version of the manuscript.

Funding: This research received no external funding.

Institutional Review Board Statement: Not applicable.

Informed Consent Statement: Not applicable.

Data Availability Statement: Due to the need for follow-up research, participants of this study did not agree for their data to be shared publicly, so supporting data are not available.

Conflicts of Interest: All authors certify that they have no affiliations with or involvement in any organization or entity with any financial or non-financial interests in the subject matter or materials discussed in this manuscript.

References

1. Meral, M.E.; Çelík, D. A comprehensive survey on control strategies of distributed generation power systems under normal and abnormal conditions. *Annu. Rev. Control* **2019**, *47*, 112–132. [CrossRef]
2. Verma, A.K.; Jarial, R.K.; Roncero-Sanchez, P.; Ungarala, M.R.; Guerrero, J.M. An Improved Hybrid Prefiltered Open-Loop Algorithm for Three-Phase Grid Synchronization. *IEEE Trans. Ind. Electron.* **2020**, *68*, 2480–2490. [CrossRef]
3. Chedjara, Z.; Massoum, A.; Wira, P.; Safa, A.; Gouichiche, A. A fast and robust reference current generation algorithm for three-phase shunt active power filter. *Int. J. Power Electron. Drive Syst. IJPEDS* **2022**, *12*, 121. [CrossRef]
4. Ahmed, H.; Çelik, D. Sliding mode based adaptive linear neuron proportional resonant control of Vienna rectifier for performance improvement of electric vehicle charging system. *J. Power Sources* **2022**, *542*, 231788. [CrossRef]
5. Safa, A.; Gouichiche, A.; Verma, A.K.; Su, C.-L.; Chedjara, Z.; Messlem, Y.; Berkouk, E.M. Open Loop Synchronization Techniques Benchmarking for Distributed Energy Sources Connection. *IEEE Access* **2022**, *10*, 63554–63566. [CrossRef]
6. Çelik, D. Lyapunov based harmonic compensation and charging with three phase shunt active power filter in electrical vehicle applications. *Int. J. Electr. Power Energy Syst.* **2022**, *136*, 107564. [CrossRef]
7. Al-Majidi, S.D.; Al-Nussairi, M.K.; Mohammed, A.J.; Dakhil, A.M.; Abbod, M.F.; Al-Raweshidy, H.S. Design of a Load Frequency Controller Based on an Optimal Neural Network. *Energies* **2022**, *15*, 6223. [CrossRef]
8. Lubura, S.; Šoja, M.; Lale, S.; Ikić, M. Single-phase phase locked loop with DC offset and noise rejection for photovoltaic inverters. *IET Power Electron.* **2014**, *7*, 2288–2299. [CrossRef]
9. Basso, T. IEEE standard for interconnecting distributed resources with the electric power system. In Proceedings of the IEEE Pes Meeting, College Station, TX, USA, 30 March–1 April 2004; p. 1.
10. Gonzalez, R.; Lopez, J.; Sanchis, P.; Marroyo, L. Transformerless Inverter for Single-Phase Photovoltaic Systems. *IEEE Trans. Power Electron.* **2007**, *22*, 693–697. [CrossRef]
11. Xiaoqiang, G.; Herong, G.; Guocheng, S. DC injection control for grid-connected inverters based on virtual capacitor concept. In Proceedings of the 2008 International Conference on Electrical Machines and Systems, Wuhan, China, 17–20 October 2008; pp. 2327–2330.
12. Armstrong, M.; Atkinson, D.J.; Johnson, C.M.; Abeyasekera, T.D. Auto-calibrating DC link current sensing technique for transformerless, grid connected, H-bridge inverter systems. *IEEE Trans. Power Electron.* **2006**, *21*, 1385–1393. [CrossRef]
13. Bowtell, L.; Ahfock, A. Direct current offset controller for transformerless single-phase photovoltaic grid-connected in-verters. *IET Renew. Power Gener.* **2010**, *4*, 428–437. [CrossRef]
14. Buticchi, G.; Lorenzani, E.; Franceschini, G. A DC Offset Current Compensation Strategy in Transformerless Grid-Connected Power Converters. *IEEE Trans. Power Deliv.* **2011**, *26*, 2743–2751. [CrossRef]
15. Guofeng, H.; Xu, D. A novel DC loop current control strategy for paralleled UPS inverter system based on decoupled control scheme. In Proceedings of the 2012 IEEE International Symposium on Industrial Electronics, Hangzhou, China, 28–31 May 2012; pp. 70–75. [CrossRef]
16. Ahfock, T.L.; Bowtell, L. DC offset elimination in a single-phase grid-connected photovoltaic system. In Proceedings of the 16th Australasian Universities Power Engineering Conference (AUPEC 2006), Melbourne, VIC, Canada, 10–13 December 2006.
17. Menniti, D.; Pinnarelli, A. A novel compensation approach for DC current component in a grid-connected photovoltaic generation system. In Proceedings of the 2012 IEEE Power and Energy Society General Meeting, San Diego, CA, USA, 22–26 July 2012. [CrossRef]
18. Song, W.; Feng, X.; Smedley, K.M. A Carrier-Based PWM Strategy with the Offset Voltage Injection for Single-Phase Three-Level Neutral-Point-Clamped Converters. *IEEE Trans. Power Electron.* **2012**, *28*, 1083–1095. [CrossRef]
19. Yan, Q.; Wu, X.; Yuan, X.; Geng, Y.; Zhang, Q. Minimization of the DC Component in Transformerless Three-Phase Grid-Connected Photovoltaic Inverters. *IEEE Trans. Power Electron.* **2014**, *30*, 3984–3997. [CrossRef]
20. Chung, D.-W.; Sul, S.-K. Analysis and compensation of current measurement error in vector-controlled AC motor drives. *IEEE Trans. Ind. Appl.* **1998**, *34*, 340–345. [CrossRef]
21. Jung, H.-S.; Hwang, S.-H.; Kim, J.-M.; Kim, C.-U.; Choi, C. Diminution of current-measurement error for vector-controlled AC motor drives. *IEEE Trans. Ind. Appl.* **2006**, *42*, 1249–1256. [CrossRef]
22. Trinh, Q.N.; Wang, P.; Tang, Y.; Choo, F.H. Mitigation of DC and Harmonic Currents Generated by Voltage Measurement Errors and Grid Voltage Distortions in Transformerless Grid-Connected Inverters. *IEEE Trans. Energy Convers.* **2017**, *33*, 801–813. [CrossRef]

23. He, G.; Xu, D.; Chen, M. A Novel Control Strategy of Suppressing DC Current Injection to the Grid for Single-Phase PV Inverter. *IEEE Trans. Power Electron.* **2014**, *30*, 1266–1274. [CrossRef]
24. Suzuki, S.; Yoshida, M. Elevator Control Apparatus with Compensation for Current Sensor Offset Voltage. U.S. Patent 5,407,027, 18 April 1995.
25. Wang, Y.F.; Li, Y.W. Grid synchronization PLL based on cascaded delayed signal cancellation. *IEE Proc. Electr. Power Appl.* **2010**, *26*, 1987–1997. [CrossRef]
26. Mellouli, M.; Hamouda, M.; Slama, J.B.H.; Al-Haddad, K. A Third-Order MAF Based QT1-PLL That is Robust Against Harmonically Distorted Grid Voltage With Frequency Deviation. *IEEE Trans. Energy Convers.* **2021**, *36*, 1600–1613. [CrossRef]
27. Du, L.; Li, M.; Tang, Z.; Xiong, L.; Ma, X.; Tang, G. A Fast Positive Sequence Components Extraction Method with Noise Immunity in Unbalanced Grids. *IEEE Trans. Power Electron.* **2019**, *35*, 6682–6685. [CrossRef]
28. Li, J.; Wang, Q.; Xiao, L.; Hu, Y.; Wu, Q.; Liu, Z. An αβ-Frame Moving Average Filter to Improve the Dynamic Performance of Phase-Locked Loop. *IEEE Access* **2020**, *8*, 180661–180671. [CrossRef]
29. Liu, X.; Wu, B.; Xiu, L. A Fast Positive-Sequence Component Extraction Method with Multiple Disturbances in Unbalanced Conditions. *IEEE Trans. Power Electron.* **2022**, *37*, 8820–8824. [CrossRef]
30. Al-Majidi, S.D.; Abbod, M.F.; Al-Raweshidy, H.S. Maximum Power Point Tracking Technique based on a Neural-Fuzzy Approach for Stand-alone Photovoltaic System. In Proceedings of the 55th International Universities Power Engineering Conference, Torino, Italy, 1–4 September 2020; pp. 1–6. [CrossRef]
31. Li, X.; Lin, H. A Design Method of Phase-Locked Loop for Grid-Connected Converters Considering the Influence of Current Loops in Weak Grid. *IEEE J. Emerg. Sel. Top. Power Electron.* **2019**, *8*, 2420–2429. [CrossRef]
32. Zhu, D.; Zhou, S.; Zou, X.; Kang, Y. Improved Design of PLL Controller for *LCL*-Type Grid-Connected Converter in Weak Grid. *IEEE Trans. Power Electron.* **2019**, *35*, 4715–4727. [CrossRef]
33. Guo, X.; Wu, W.; Chen, Z. Multiple-Complex Coefficient-Filter-Based Phase-Locked Loop and Synchronization Technique for Three-Phase Grid-Interfaced Converters in Distributed Utility Networks. *IEEE Trans. Ind. Electron.* **2010**, *58*, 1194–1204. [CrossRef]
34. Karimi-Ghartemani, M.; Iravani, M.R. A Method for Synchronization of Power Electronic Converters in Polluted and Variable-Frequency Environments. *IEEE Trans. Power Syst.* **2004**, *19*, 1263–1270. [CrossRef]
35. Teodorescu, R.; Liserre, M.; Rodríguez, P. Grid synchronization in threephase power converters. In *Grid Converters for Photovoltaic and Wind Power Systems*; IEEE: Piscataway, NJ, USA, 2007; pp. 169–204.
36. Jin, N.; Gan, C.; Guo, L. Predictive Control of Bidirectional Voltage Source Converter with Reduced Current Harmonics and Flexible Power Regulation Under Unbalanced Grid. *IEEE Trans. Energy Convers.* **2017**, *33*, 1118–1131. [CrossRef]
37. Nishiyama, K. A nonlinear filter for estimating a sinusoidal signal and its parameters in white noise: On the case of a single sinusoid. *IEEE Trans. Signal Process.* **1997**, *45*, 970–981. [CrossRef]
38. Dash, P.; Panda, G.; Pradhan, A.; Routray, A.; Duttagupta, B. An extended complex Kalman filter for frequency measurement of distorted signals. *EEE Trans. Instrum. Meas.* **2002**, *49*, 746–753. [CrossRef]
39. Dash, P.K.; Pradhan, A.K.; Panda, G. Frequency estimation of distorted power system signals using extended complex Kalman filter. *IEEE Trans. Power Deliv.* **1999**, *14*, 761–766. [CrossRef]
40. Huang, C.-H.; Lee, C.-H.; Shih, K.-J.; Wang, Y.-J. Frequency Estimation of Distorted Power System Signals Using a Robust Algorithm. *IEEE Trans. Power Deliv.* **2007**, *23*, 41–51. [CrossRef]
41. Ahmed, K.; Massoud, A.; Finney, S.; Williams, B.J.I.P.E. Autonomous adaptive sensorless controller of inverter-based islanded-distributed generation system. *IET Power Electron.* **2009**, *2*, 256–266. [CrossRef]
42. Andrew, E.T.; Ahmed, K.H.; Holliday, D. A New Model Predictive Current Controller for Grid-Connected Converters in Unbalanced Grids. *IEEE Trans. Power Electron.* **2022**, *37*, 9175–9186. [CrossRef]
43. El-Nagar, M.; Elattar, O.; Ahmed, K.; Hamdan, E.; Abdel-Khalik, A.S.; Hamad, M.S.; Ahmed, S. Space vector-based model predictive current controller for grid-connected converter under unbalanced and distorted grid without a phase-locked loop. *Alex. Eng. J.* **2023**, *77*, 265–281. [CrossRef]
44. Pérez-Guzmán, R.E.; Rivera, M.; Wheeler, P.W. Recent advances of predictive control in power converters. In Proceedings of the 2020 IEEE International Conference on Industrial Technology (ICIT), Buenos Aires, Argentina, 6–28 February 2020; pp. 1100–1105.